Standing/Walking Stabilization of Humanoid Robot
by Visual Servoing Concept through Online-Visual-Pose-Estimation

Wei Song[1], Tomohide Maeba[2], Geng Wang[2], Mamoru Minami[2] Akira Yanou[2] and Yanan Zhang[1]

[1]School of Mechatronics Engineering and Automation, Shanghai University, Shanghai, China
(Tel: +86-21-5633-1783; E-mail: songwei5726@hotmail.com)
[2]Graduate School of Natural Science and Technology, Okayama University, Okayama, Japan
(Tel: +81-86-252-1111; E-mail: minami@qumi.sys.okayama-u.ac.jp)

Abstract: Although many papers have been published on visual tracking, visual servoing of the vision-based robotics, there are only few research study on using vision to improve the standing and walking stabilization for legged robots. In this paper, we set two cameras as the humanoid's eyes, to observe a static object in front, and using the visual measured information to control the robot keeping a desired head-top's position/orientation, in order to help the robot to prevent from unstable motion, such as the falling down action caused by gravity or dangerous slipping motion happened suddenly.

Keywords: humanoid, stable standing/walking, visual servoing concept.

1. INTRODUCTION

Humanoid robots are complex autonomous control systems that involve many technical issues to be solved, among which stable biped walking is the most fundamental, therefore it has been researched widely and a number of control approaches have been proposed to advance walking reliability.

The zero-moment-point (ZMP) approach is extensively utilized and has been shown that can provide robust and effective locomotion for biped robots [1], [2]. The works using ZMP should firstly design a desired trajectory off-line, then derive the body motion based on it. Since the natural dynamics of the robots is not considered, the ZMP methods often result in unnatural-looking gait. Moreover, not every desired ZMP trajectory can be achieved because of robot's kinematical limitation. In researches [3] and [4] ZMP is not used, but the robot walking has also been achieved by finding dynamically stable trajectories of joints through inverse kinematics calculations in advance from e.g., body's desired trajectory. This trajectory tracking approach is stable by following predetermined walking gaits, but it is difficult to realize adaptive walking in a complicated environment with unknown disturbances, where robots may encounter unpremeditated contact with e.g. furniture, humans, or irregularities of a ground.

Therefore some online control methods for making the walking control system stable against such disturbances have been intensively researched so far. Among them, walking control based on reflexive action is a method using sensory information to help the robot adapt to a time-changing environment. Qiang Huang et al. [5] have proposed a gait control consisting of a feedforward dynamic pattern and a feedback sensory reflex, which enabled a humanoid to effectively walk on unknown rough terrain and in an environment with disturbances. The sensory devices used in [5] include a foot-force sensor, the body-inclination sensors, and joint encoders.

As one of the most important sensory, vision has been used in lots of robot control research field, such as visual tracking and visual servoing. However, there are only few research study on using vision to improve the standing and walking stabilization for legged robots. In this research, we newly propose a "Visual Lifting Bipedal Walking" strategy, which uses the vision sensory reflex to deal with the stabilization of the humanoid robot's biped standing and walking, as shown in Fig.1.

One of the problems that has not been solved for online bipedal walking control is concerning a singularity of Jacobean matrix that happens in robot's walking. This problem occurs because the Jacobean matrix is determined as a function of the robot's shape that is a result of the online dynamical motion to avoid unpredictable disturbances, so it cannot be prevented with some preparation. Since this problem lying in stable walking standing against online adaptiveness is naturally influenced by unpredictable disturbances, some researchers start to work on how to retain the stability, e.g. [6], [7]. Considering one of the hazardous restrictions that the singularity of Jacobean matrix J connecting velocity vector in Cartesian space and joint velocity vector, which prohibits the calculation of $\dot{q} = J(q)^{-1}\dot{r}$, in this paper, we proposed to use Jacobean transpose $J(q)^T$, which has an ability to project the force and torque exerting on the robot onto each joint space that is basically free from the singularity. On the other hand, human looks like using the singular configuration to walk despite the above difficulties, making human's walking posture upright. On this view point, the strategy of utilizing $J(q)^T$ may have wider potential than $J(q)^{-1}$ to help the robot realize human-like walking.

In this paper we propose Visual Lifting Stable Walking scheme based on a visual servoing concept. We use cameras as the humanoid's eyes, to observe a static object that is set in the right front to measure the robot's head pose based on the object through visual pose estimation ([8],[9]) during walking or just standing. $J(q)^T$ is used in our research to project stabilizing force and
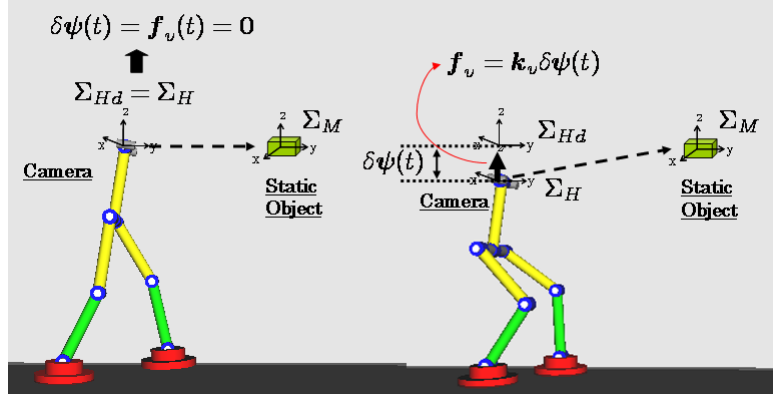
Fig. 1 Visual Lifting Bipedal Walking Strategy

torque that is calculated by visual measurement onto each joint, exemplifying the possibility for stable walking by using a dynamical model including various walking gait patterns. The decreased robot head may lead to falling to the ground, therefore we use the pose deviation from a desired head pose (height and orientation) to deduce a pulling force of head by using joint torques, which are calculated through the Jacobine-transpose and lifting force desired by the detected head pose sinking deviation. We will introduce this strategy in the following section.

2. VISUAL LIFTING BIPEDAL WALKING STRATEGY

Here, we use two cameras that are set as the humanoid's eyes to measure the pose of a object being set stationarily in the right front, to perform vision-feedback control for improving humanoid's standing/walking stability.

We use a model-based matching method to measure the pose of a target object denoted by ψ based on a moving coordinates Σ_H, which represents the robot's head. we use a "1-step GA" method to solve the model matching optimization problem to realize online visual pose estimation [8].

The desired relative pose of Σ_M (target object coordinate) and Σ_H is predefined by Homogeneous Transformation as $^{Hd}\boldsymbol{T}_M(t)$. The difference of the desired head pose Σ_{Hd} and the current pose Σ_H is denoted as $^H\boldsymbol{T}_{Hd}$, it can be described by

$$^H\boldsymbol{T}_{Hd}(\delta\boldsymbol{\psi}(t)) = {}^H\boldsymbol{T}_M(\hat{\boldsymbol{\psi}}(t)) \, {}^{Hd}\boldsymbol{T}_M^{-1}(\boldsymbol{\psi}_d(t)), \quad (1)$$

where $^H\boldsymbol{T}_M(t)$ is calculated by $\hat{\boldsymbol{\psi}}(t)$ that is measured by online visual pose estimation method.

Here, the force exerted on the head to minimize the difference of the desired head pose and the current pose $^H\boldsymbol{T}_{Hd}$ —the pose deviation of the robot's head caused by gravity force and walking dynamical influences— is considered to be directly proportional to $\delta\boldsymbol{\psi}(t)$, so we have

$$\boldsymbol{f}_v = \boldsymbol{k}_v \delta\boldsymbol{\psi}(t). \quad (2)$$

The above Visual Lifting Bipedal Walking strategy is depicted in Fig. 1.

The joint touque and force $\boldsymbol{\tau}_v$ to be input to realize $\boldsymbol{f}_v$ at the head has following relation [10]

$$\boldsymbol{\tau}_v = \boldsymbol{J}_v^T \boldsymbol{f}_v, \quad (3)$$

where $\boldsymbol{J}_v$ is a Jacobian matrix of the head pose against joint angles. We use $\boldsymbol{\tau}_v$ to control the humanoid robot keeping stable standing/walking, by compensating the falling down action caused by gravity or dangerous slipping motion happened unpredictably etc. by using the visual feedback information. Simulation will be conducted to confirm the effectiveness of our proposed control method, and the result will be shown later in this paper.

3. BIPEDAL WALKING MODEL

3.1 Dynamics of Walking

The humanoid robot consists of a body, legs, and eyes, which has 10 degrees of freedom. Each link has mass m, length l, radius of link r, and inertia moment I, and each joint has viscous friction D.

Here as a fundamental research we set conditions that the angles of bady and legs rotate around x direction of Σ_W. When the robot walks forward, the robot is getting closer to the static target object, so it is necessary to change the pose of the cameras to keep the object always in both views of the left and right cameras. Therefore, there are angles to rotate cameras around z direction of Σ_W to change eyes' gazing direction.

The equations of motion that includes point-constraint condition including contacting friction is written as

$$\boldsymbol{M}(\boldsymbol{q})\ddot{\boldsymbol{q}} + \boldsymbol{h}(\boldsymbol{q}, \dot{\boldsymbol{q}}) + \boldsymbol{g}(\boldsymbol{q}) + \boldsymbol{D}\dot{\boldsymbol{q}}$$
$$= \boldsymbol{\tau} + \{(\frac{\partial C}{\partial \boldsymbol{q}^T})^T / \|\frac{\partial C}{\partial \boldsymbol{r}^T}\|\}f_n - (\frac{\partial \boldsymbol{r}}{\partial \boldsymbol{q}^T})^T \frac{\dot{\boldsymbol{r}}}{\|\dot{\boldsymbol{r}}\|} f_t. \quad (4)$$

$\boldsymbol{M}$ is inertia matrix, $\boldsymbol{h}$ and $\boldsymbol{g}$ indicate Coriolis force, centrifugal force and gravity, $\boldsymbol{D}$ is matrix that indicates coefficients of joints' viscous friction. $\boldsymbol{q}$ is joint angle and $\boldsymbol{\tau}$ is input torque. Then, f_n is constraint force and f_t is friction. Here, we set two reasonable assumptions: (i) f_n and f_t are orthogonal. (ii) $f_t = Kf_n$ (K is proportional constant).

In addition, C is defined as point-constraint condition $C(\boldsymbol{r}(\boldsymbol{q})) = 0$, where $\boldsymbol{r}(\boldsymbol{q})$ is lifting foot's pose vector.
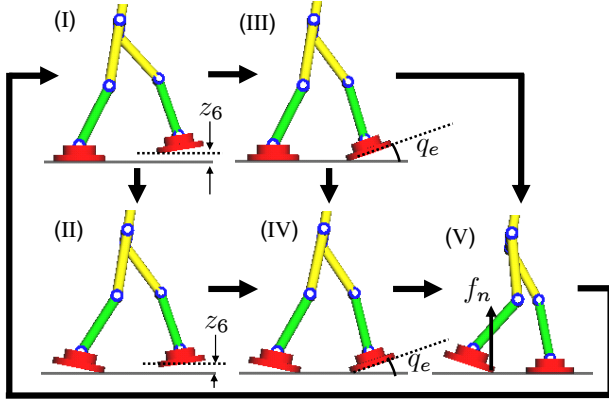
Fig. 2 Style transition diagram for bipedal walking

This constraint condition happens to appear when the lifting foot's z-position in Σ_W being zero or below zero, otherwise the second and third terms of right-hand side of Eq.(4) disappear. The constraint condition concerning $\ddot{q}$ given by differentiating $C(r(q)) = 0$ by two times is written as

$$\dot{q}^T\{\frac{\partial}{\partial q}(\frac{\partial C}{\partial q^T})\}\dot{q} + (\frac{\partial C}{\partial q^T})\ddot{q} = 0. \tag{5}$$

Abbreviating the coefficient vectors of f_n and f_t in Eq.(4) by j_c^T and j_t^T, Eq.(4) and Eq.(5) can be combined as follows.

$$\begin{bmatrix} M(q) & -(j_c^T - j_t^T K) \\ \frac{\partial C}{\partial q^T} & 0 \end{bmatrix} \begin{bmatrix} \ddot{q} \\ f_n \end{bmatrix}$$
$$= \begin{bmatrix} \tau - h(q,\dot{q}) - g(q) - D\dot{q} \\ \dot{q}^T\{\frac{\partial}{\partial q}(\frac{\partial C}{\partial q^T})\}\dot{q} \end{bmatrix}. \tag{6}$$

Because the size of matrix $M(q)$ is generally very large, compelling a large amount of computation to calculate each element of $M(q)$ by using Lagrange method. In our research, we have 10 links, so $M(q)$ is a 10×10 matrix. This implies that analytical deriving of Eq.(4) is almost impossible by hand writing calculation. A "Newton-Euler" method introduced in [11] can calculate such kinds of dynamical coefficients numerically and recursively through forward dynamics calculation. So we use this method in our simulation.

3.2 Walking Style Representation

The walking sequence of the flat-foot is more complicated than those of the point-foot and the round-foot, because each flat-foot has three contact cases: heel-contact, toe contact and foot contact. As shown in Fig. 2, there are several walking styles (I), (II), $\cdots$ (V) in the walking sequence. A walking process may not include all these styles, moving from which one to which phase of the motion depends on the equation of motion and some predefined conditions i.e. shape of the ground, size of foot and so on. All dynamical parameters can affect the resulted motion of walking gait's variety.

Let the forward leg be expressed by "FL" and the backward leg be expressed by "BL", we can describe the characteristics of each walking style as follows.

Style I: Surface-contacting (BL)

Link-0 is surface-contacting without slipping, being regarded as a part of ground.

Style II: Point-contacting (BL)

Link-0 is point-contacting, but constraint condition about Link-0 need not to be incorporated like Eq.(4), that is, the second and third terms should be eliminated, since the motion of Link-0 can be added to the equation of motion as additional state q_0, setting the number of states of Eq.(6) increase by one.

Style III: Surface-contacting (BL) and point-contacting (FL)

The heel of FL (tip of Link-6) is point-contacting, and BL is surface-contacting which is the same with (I). The constraint condition is required for the heel of FL.

Style IV: Point-contacting for both (BL) and (FL)

The heel of FL (tip of Link-6) is point-contacting, and Link-0 is rotating which is the same with (II). The constraint condition is required for the heel of FL and angle of Link-0 should be considered. In this case, the left-hand side of Eq.(4) is identical to the one of Stale II.

Style V: Point-contacting (BL) and surface-contacting (FL)

In this walking style, FL becomes surface-contacting, being regarded as a part of ground. BL is point-contacting under constraint condition. The backward leg can be used for exerting torque by ankle.

3.3 Thansition Conditions among Phases
(1): from (I) to (II) and from (III) to (IV)

This change of phase means that the heel of the rear-foot detaches from the ground in Phase (I) or (III). Firstly, reference coordinate of $^1f_1$ (exerting torque to Link-1 whose vector is represented by a coordinates Σ_1 being fixed at Link-1) and $^1n_1$ (exerting torque to Link-1 as the same manner like $^1f_1$) is converted from Σ_1 to Σ_W by $^Wf_1 = {}^WR_1{}^1f_1$ and $^Wn_1 = {}^WR_1{}^1n_1$.

Then, projection to z-axis, meaning a vertical axis of the ground of $^Wf_1 = [{}^Wf_{1x}, {}^Wf_{1y}, {}^Wf_{1z}]^T$ and projection to x-axis, representing a rotational axis of foot of $^Wn_1 = [{}^Wf_{1x}, {}^Wf_{1y}, {}^Wf_{1z}]^T$ are derived by using unit vector $e_x = [1, 0, 0]^T$ and $e_z = [0, 0, 1]^T$, as

$$^Wf_{1z} = e_z^T \, {}^Wf_1 \tag{7}$$
$$^Wn_{1x} = e_x^T \, {}^Wn_1 \tag{8}$$

Given that the foot contacts with the ground at two representative points of heel and tiptoe, $^Wf_{1z}$ and $^Wn_{1x}$ are dispersed and act on both ends of Link-0.

Here, when resultant forces that act on rear/front of Link-0 are defined as F_R and F_F respectively, we can get

Table 1 Physical parameters values in simulations

Link Number	0	1	2	3
Mass m_i [kg]	1.0	1.0	1.0	1.5
Length l_i [m]	0.5	2.0	2.0	1.5
Radius r_i [m]	(0.8, 0.5)	0.2	0.2	0.2

Link Number	5	6	7	8
Mass m_i [kg]	1.0	1.0	3.0	1.0
Length l_i [m]	2.0	0.5	2.0	0.5
Radius r_i [m]	0.2	(0.5, 0.8)	0.2	0.5

two equations below.

$$F_R = \frac{{}^W f_{1z}}{2} + \frac{{}^W n_{1x}}{L} \qquad (9)$$

$$F_F = \frac{{}^W f_{1z}}{2} - \frac{{}^W n_{1x}}{L} \qquad (10)$$

Thus, when the value of F_R becomes negative, Link-0 begins to rotate around the tiptoe, which means the heel detaches from the ground. For this reason, inequality $F_L < 0$ is condition expression for switching.

(2): from (I) to (III) or from (II) to (IV)

When the heel of forefoot attaches the ground, the phase is switched from (I) to (III) or from (II) to (IV). Therefore, given z axis of the forefoot's heel is defined as z_6, switching condition is $z_6 \leq 0$.

(3): from (III) to (V) or from (IV) to (V)

When Link-6, defined as a lifting foot's link, becomes surface-contacting, the phase is switched from (III) to (V) or from (IV) to (V). That is, when $q_e(= q_0 + q_1 + \cdots + q_6)$ is defined as angle between Link-6 and the ground shown in Fig. 2, switching condition is $q_e \leq 0$.

(4): from (V) to (I)

When a condition that tiptoe (the tip of Link-6′, which is renamed into Link-6′ for the name of Link-6 in phase of (III) or (IV) since the robot's basic configuration of (V) and (I) are identical but the link's numbers are vice versa derived from left leg and right leg being reversed) detaches from the ground is satisfied, phase (V) is switched to phase (I). In this posture, constraint force f_n acts on Link-6′. That is, if the value of f_n is positive, Link-6′ contacts with the ground. Meanwhile, if the value of f_n is negative, Link-6′ starts lifting, then the condition is $f_n < 0$.

4. SIMULATION RESULTS

We perform simulations to verify the effectiveness of the proposed visual lifting bipedal walking method. Graphic presentation of robot's motion is conducted by "Open GL", as shown in Fig. 3, and the robot's parameter values used in the following analyse are shown in Table 1.
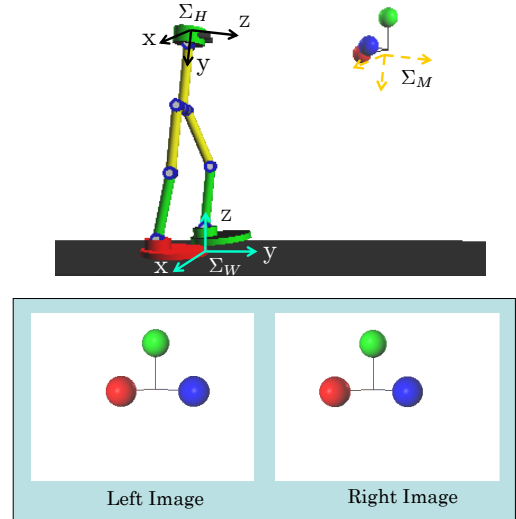
Fig. 3 Visual lifting bipedal robot simulation system.

4.1 Standing Simulation with "Visual Lifting"

Here, to show the effectiveness of the "Visual Lifting" ability to help the robot to stand, we firstly let the robot stand without visual feedback. We can image that without "Visual Lifting", the robot will be falling to the ground due to the gravity. The results are shown in Fig. 4. The values of ${}^W y_H$ in Fig. 4(b) is increasing and the values of ${}^W z_H$ in Fig. 4(c) is decreasing gradually, which means the trajectory of the robot's head turns to forward and fall to the ground, so the robot failed to stand without visual feedback.

The "Visual Lifting" bipedal robot system is shown in Fig. 3, we use a 3D marker that is composed by red, blue, green balls as the target object, which is located in front of the bipedal robot and static in this simulation. The object'pose is measured on-line by a proposed model-based evolutionary method [8]. The measured results are used to deduce a pulling force to control the robot to keep a standing motion, the strategy has been explained in Section 2. The results are shown in Fig. 5. Compared with the Fig. 4(b) and (c), the values of ${}^W y_H$ and ${}^W z_H$ are not increasing/decreasing all the time, the changing are curve lines, which means the robot's head swings around the desired position. Figures 6 and 7 are shown the recognition results during the standing performance. Figure 6 is the fitness function value that represents the measurement accuracy. During 2.7[s] to 3[s], the fitness function value is decreased to zero, which means the robot's head moves far away from the start location at this time, resulting in the object's pose gets out of the recogntion range. Figure 7 (a) (b) and (c) show the postion measured results, and (d) shows the orientation measured results.

By comparing this two simulations, we can give the conclusion that the proposed "Visual Lifting" robot control scheme based on visual servoing concept is effective to prevent from falling to the ground against the gravity while the robot is standing. However, the simulation results show the standing with visual feedback is not stable, the robot's head swings around a desired position. We
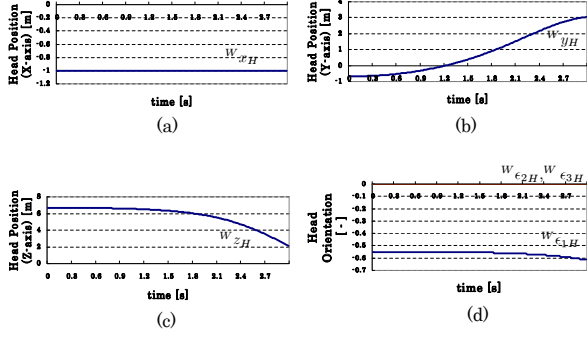
Fig. 4 Head pose values while standing without visual feedback. (a) Hand position values in x-axis of Σ_W. (b) Hand position values in y-axis of Σ_W. (c) Hand position values in z-axis of Σ_W. (d) Hand orientation values in Σ_W, expressed by $^W\epsilon_{1H}, ^W\epsilon_{2H}, ^W\epsilon_{3H}$.
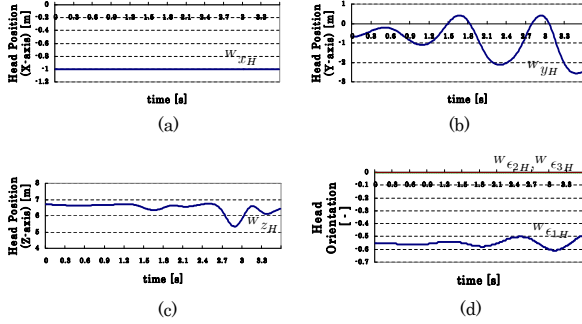
Fig. 5 Head pose values while standing with visual feedback. (a) Hand position values in x-axis of Σ_W. (b) Hand position values in y-axis of Σ_W. (c) Hand position values in z-axis of Σ_W. (d) Hand orientation values in Σ_W, expressed by $^W\epsilon_{1H}, ^W\epsilon_{2H}, ^W\epsilon_{3H}$.

consider one of the reasons is that the pull force is conculated by only the pose error (Eq.(2)), that is, we only consider the robot's pose for controlling, the velocity is not under consideration, so the swing motion happens and con not be converged to the desired pose.

4.2 Walking Simulation under Correct Visual Measurement Assumption

Here, to evaluate the "visual lifting" ability in bipedal walking performance, we assume the visual measurement is correct, including no error. That is, the values of $^E\boldsymbol{T}_M(\hat{\boldsymbol{\psi}}(t))$ in Eq. (1) is calculated based on the camera position given by the robot kinematics, with the object position in Σ_W given in advance.

We set $\boldsymbol{k}_v = (150, 150, 150)$. Figure. 8 is the head trajectory of y-coordinate (walking direction) and z-coordinate (upright direction) values that are normalized by body height. Figure. 8 (a) shows that the robot is walking forward with a distance of 0.6 (body height) in 10[s], (b) shows that the head height is decreasing during walking from 1 to 0.85 (body height), and the height has been retained during walking. Figure. 9 (a) shows how
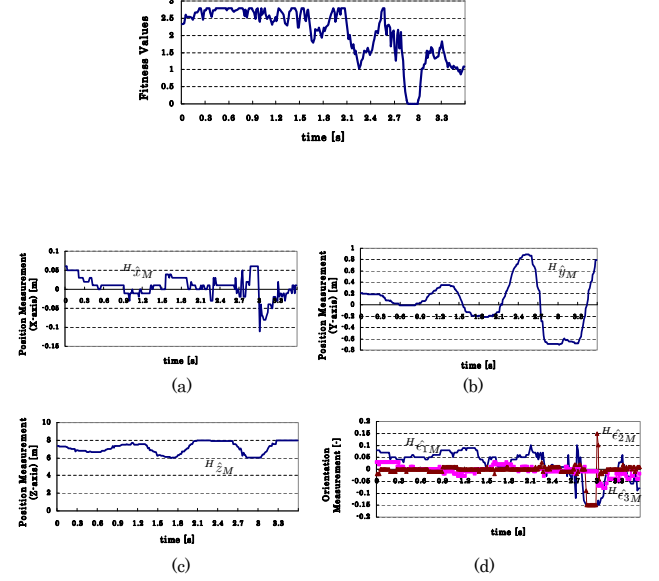
Fig. 7 Measurement result in "visual lifting" control : (a) Object position values in x-axis of Σ_H. (b) Object position values in y-axis of Σ_H. (c) Object position values in z-axis of Σ_H. (d) Object orientation values in Σ_H, expressed by $^H\hat{\epsilon}_{1M}, ^H\hat{\epsilon}_{2M}, ^H\hat{\epsilon}_{3M}$

.

walking style changes in this situation. It is a rhythmic motion that each one is changing by Style I − > Style III − > Style V with a period of 0.9[s]. Figure. 9 (b) is foot trajectory on the ground. We can calculate the average length of one walking step is about 0.145 body height. Figure. 10 shows the leg trajectory expressed by phase portrait: the relation of thigh angle (the angle between two legs) and its velocity. Since the initial posture is thigh angle is 0[rad], the single line from 0[rad] to 0.9[rad] represents the first step of the walking that performed by one leg, then the other leg follows but does not move over the first one, so the thigh angle decreased to about 0.6[rad]. Then another walking cycle starts, first step is from 0.6[rad] to 1.2[rad], second step from 1.2[rad] return to about 0.6[rad], the following gaits appeared in the same manner.

The simulation of Visual Lifting Bipedal Walking in the way of Style I − > Style III − > Style V is shown in Fig. 11.

5. CONCLUSION

In this paper, we proposed a "Visual Lifting Bipedal Walking" strategy, by using the visually measured information to control the robot for keeping a desired head-top's position/orientation to avoid falling down.

Simulations has been performed to present the effectiveness of "visual lifting" ability. It has been confirmed that the proposed method is effective to prevent from falling to the ground against the gravity while the robot is standing. And by assuming the visual measurement is correct, we performed the simulation of Visual Lifting Bipedal Walking, the walking styles changed as Style I − > Style III − > Style V.
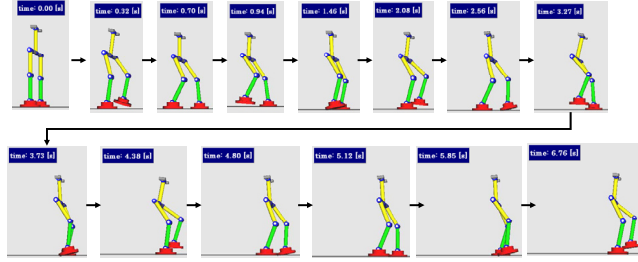
Fig. 11 Visual Lifting Bipedal Walking, Style I –> Style III –> Style V.
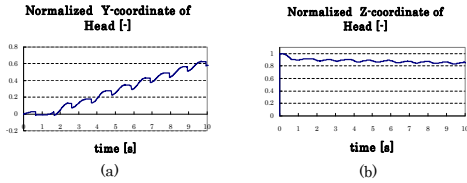
Fig. 8 Head trajectory of y-coordinate and z-coordinate in the case of $\boldsymbol{k}_v = (150, 150, 150)$. Both y-coordinate and z-coordinate values are normalized by body height.
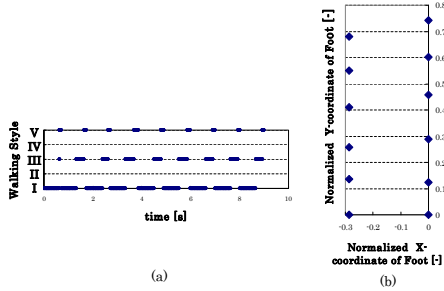
Fig. 9 (a)Step changing with respect to time. (b)Foot trajectory on the ground. This simulation is in the case of $\boldsymbol{k}_v = (150, 150, 150)$. Both x-coordinate and y-coordinate values are normalized by body height. From (b) we can calculate the average length of
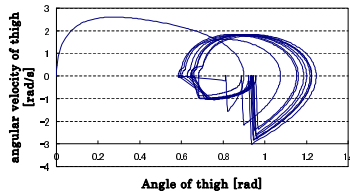
Fig. 10 Leg trajectory of the dynamic walking, expressed by phase portrait, in the case of $\boldsymbol{k}_v = (150, 150, 150)$.

However, the simulation results show the standing with visual feedback is not stable, the robot's head swings around a desired position. We consider one of the reasons is that the pull force is conculated by only the pose error (Eq.(2)), that is, we only consider the robot's pose for controlling, the velocity is not under consideration, so the swing motion happens and con not be converged to the desired pose. In the future work, we will deal with this unstable problem, try to make the robot perform an

effective and stable walking by "visual lifting" with on-line measurement.

REFERENCES

[1] D. Djoudi, C. Chevallereau, and J. Grizzle, *A path-following approach to stable bipedal walking and zero moment point regulation*, in Proc. IEEE Int. Conf. Robot. Autom., Rome, Italy, 2007, pp. 3597-3602.

[2] C. Chevallereau, D. Djoudi, and J. Grizzle, *Stable bipedal walking with foot rotation through direct regulation of the zero moment point*, IEEE Trans. Robot., vol. 25, no. 2, pp. 390-401, Apr. 2008

[3] J. Yamaguchi, S. Inoue, D. Nishino, and A. Takanishi, *Development of a bipedal humanoid robot having antagonistic driven joints and three dof trunk*, in Proc. of the 1998 IEEE/RSJ Int. Conf. on Intelligent Robots and Systems, pp. 96101, 1998.

[4] K. Nagasaka, M. Inaba, and H. Inoue, *Walking pattern generation for a humanoid robot based on optimal gradient method*, in proceeding of IEEE Int. Conf. on Systems, Man, and Cybernetics, 1999.

[5] Qiang Huang and Yoshihiko Nakamura, *Sensory Reflex Control for Humanoid Walking*, IEEE Trans. Robot., vol. 21, no. 5, pp. 977-984, Oct. 2005.

[6] K. Nishiwaki and S. Kagami, *Online walking control system for humanoids with short cycle pattern generation*, The International Journal of Robotics Research, vol. 28, no. 6, pp. 729742, 2009.]

[7] Koichi Nishiwaki and Satoshi Kagami, *Online Design of Torso Height Trajectories for Walking Patterns that takes Future Kinematic Limits into Consideration*, IEEE Int. Conf. on Robotics and Automation, pp. 2029-2034, 2011].

[8] Wei SongMamoru Minami, Fujia Yu, Yanan Zhang and Akira Yanou, *3-D Hand & Eye-Vergence Approaching Visual Servoing with Lyapunouv-Stable Pose Tracking*, IEEE Int. Conf. on Robotics and Automation (ICRA), pp.5210-5217, 2011.

[9] E. Mails, *Improving vision-based control using efficient second-order minimization techniques* in Proceedings of IEEE International Conference on Robotics and Automation, pp. 1843-1848, 2004.

[10] Tsuneo Yoshikawa, *Foundations of Robotics*, MIT Press, 1990.

[11] Tsutomu Mita, Koichi Osuka, *Introduction to Robot Control*, ISBN 4-339-03137-2, 1989.